

Sharp 2E upconversion luminescence of Cr^{3+} in $\text{Y}_3\text{Ga}_5\text{O}_{12}$ codoped with Cr^{3+} and Yb^{3+}

S. Heer, M. Wermuth, K. Krämer, and H. U. Güdel*

Department of Chemistry and Biochemistry, University of Bern, 3000 Bern 9, Switzerland

(Received 6 September 2001; published 14 March 2002)

We report on upconversion luminescence in $\text{Y}_3\text{Ga}_5\text{O}_{12}$ codoped with Cr^{3+} and Yb^{3+} . This is, to our knowledge, the first upconversion process directly involving Cr^{3+} . At low temperature excitation around $10\,314\text{ cm}^{-1}$ leads to relatively strong red luminescence in the title compound. The sharp upconversion luminescence around $14\,300\text{ cm}^{-1}$ is identified as the ${}^2E \rightarrow {}^4A_2$ transition of Cr^{3+} . The upconversion excitation spectrum follows the $\text{Yb}^{3+} {}^2F_{7/2} \rightarrow {}^2F_{5/2}$ absorptions in the range $11\,200\text{--}10\,315\text{ cm}^{-1}$. From transient measurements the upconversion mechanism is found to be dominated by an energy transfer step: Two excited Yb^{3+} ions simultaneously transfer their excitation energy to the Cr^{3+} ion. In $\text{Y}_3\text{Ga}_5\text{O}_{12}:2\% \text{Cr}^{3+}, 1\% \text{Yb}^{3+}$ the efficiency of the process at 10 K and for 150 mW laser power is 6% and decreases with increasing temperature due to intrinsic loss mechanisms of the system.

DOI: 10.1103/PhysRevB.65.125112

PACS number(s): 78.55.-m, 42.79.Nv, 78.20.-e

I. INTRODUCTION

One possibility to convert long-wavelength radiation into shorter-wavelength radiation is by the photophysical phenomenon of a so-called photon upconversion (UC) process. Especially in the field of generating visible (VIS) radiation by near-infrared (NIR) pump sources, the upconversion process has become important in recent years since strong NIR diode lasers became available. Several lasers,¹ imaging material devices,² and IR quantum counting devices³ have been reported based on UC pumping mechanisms. Thus design and characterization of solid-state materials that show NIR-to-VIS upconversion is an attractive and relevant research field.

In the field of NIR-to-VIS upconversion the main interest is centered on UC materials containing lanthanides since these have various excited states from which luminescence may originate. The much younger research field of transition-metal upconversion has grown in recent years but is much less explored. UC has been observed in Ti^{2+} ,⁴ Ni^{2+} ,⁵ Mo^{3+} ,⁶ Re^{4+} ,⁷ and Os^{4+} (Ref. 8) doped systems. The major advantage of the transition-metal ions over rare-earth ions is their sensitivity towards the ligand-field environment. On the other hand, multiphonon relaxation processes are much more competitive in transition-metal-ion-doped crystals and glasses, leading to important loss processes. As a result, multiple excited-state emission and upconversion phenomena are very rare. The idea to combine the different spectroscopic properties of rare-earth and transition-metal ions for new UC materials is promising. Very recently, Yb^{3+} -sensitized Mn^{2+} upconversion has been observed in Yb^{3+} -doped RbMnCl_3 ,^{9,10} CsMnCl_3 ,^{10,11} and CsMnBr_3 .¹²

In the following text we report on the spectroscopic properties of $\text{Y}_3\text{Ga}_5\text{O}_{12}$ (YGG) codoped with Cr^{3+} and Yb^{3+} . A great deal of attention has been devoted to the light-emission properties of Cr^{3+} in a big variety of crystal and glassy environments. Garnets are well-known host lattices for many dopant ions. They have the general formula $A_3B_2C_3O_{12}$ and

crystallize in the cubic space group $Ia\bar{3}d$.¹³ The unit cell contains eight formula units. A is a dodecahedrally, B an octahedrally, and C a tetrahedrally coordinated site with point symmetries D_2 , S_6 , and S_4 , respectively. In $\text{Y}_3\text{Ga}_5\text{O}_{12}$ crystals, the large Y^{3+} ions occupy the A and the Ga^{3+} ions the B and C sites. The impurity ions Cr^{3+} and Yb^{3+} are expected to substitute for the Ga^{3+} on the B and the Y^{3+} on the A sites, respectively. The octahedrally coordinated B site is weakly trigonally distorted along the diagonals of the unit cells. The distorted octahedra are surrounded antiprismatically by six edge-sharing dodecahedra. Whereas the BO_6 octahedra are isolated from each other, the dodecahedra are not: They are connected via four edges to other dodecahedra.

This paper reports on the observation of relatively strong, sharp $\text{Cr}^{3+} {}^2E \rightarrow {}^4A_2$ luminescence upon NIR $\text{Yb}^{3+} {}^2F_{5/2}$ excitation in YGG: Cr^{3+} , Yb^{3+} . With the exception of our brief communication¹⁴ it is the first report on an upconversion process directly involving Cr^{3+} . We present experimental results, propose a mechanism for the observed UC process, and describe the intrinsic loss mechanisms that are active in the title compounds.

II. EXPERIMENT

A. Crystal growth

Single crystals of YGG:Cr, YGG:Yb, and YGG:Cr, Yb with three different Cr and equal Yb concentrations, were grown by the flux technique.¹⁵ A 3:5 molar ratio of high-purity Y_2O_3 (99.9999%, Johnson & Matthey) and Ga_2O_3 (99.995%, Chempur) were used as starting materials. Doping with Yb^{3+} and Cr^{3+} was achieved by adding defined amounts of Yb_2O_3 (99.9999%, Ultrafunction Enterprises & Co.) and $\text{Cr}(\text{NO}_3)_3 \cdot 9\text{H}_2\text{O}$ (99.999%, Alfa Johnson & Matthey). In all syntheses Bi_2O_3 (99.9995%, Chempur) was added to the mixture of the starting materials in a ratio 9:1 as a flux medium. The reaction mixture was filled in 30 or 50 ml platinum crucibles closed by a platinum lid. The crucibles were placed in a corundum tube that was introduced in a SiC furnace for heating. The furnace was heated to $1300\text{ }^\circ\text{C}$ to

melt the Bi_2O_3 flux and to dissolve the starting materials. The resulting melt was homogenized for 24 h at 1300 °C. The furnace was cooled from 1300 to 1000 °C with a slow rate of 0.02 K/min to achieve nucleation and initial growth of crystals. Further growth was performed by cooling from 1000 to 800 °C at a rate of 0.5 K/min. Finally the crystals were cooled to room temperature.

By this synthetic method and under the conditions described above, we obtained a small number (3–8) of single crystals with dimensions around 1–10 mm. Crystals doped with Cr^{3+} were light to dark green depending on the concentration. In all the Cr^{3+} -doped crystals a concentration gradient was observed. The borders of the crystals were slightly brownish, which is most probably due to the incorporation of Bi^{3+} from the flux. The crystals doped with Yb^{3+} were transparent, except for the brownish color mentioned above.

The actual Cr and Yb concentrations (mol% per site) of the resulting crystals were determined by inductively coupled plasma (ICP) elemental analysis and were YGG:2% Cr, 1% Yb, YGG: 5% Cr, 1% Yb, YGG:14% Cr, 1% Yb, YGG:2% Cr, and YGG:1% Yb. Additionally, we determined the Bi and Er impurity concentrations that were around 1–2% and <0.001%, respectively, in all the samples. The ICP method cannot distinguish between valence states of the ions, but since we have no direct spectroscopic evidence for other valence states, we ascribe the concentrations to Cr^{3+} , Yb^{3+} , Er^{3+} , and Bi^{3+} . All the samples were characterized by x-ray powder diffraction. They are single-phase cubic materials, space group $Ia3d$ with $a=12.28$ Å. A crystal of YGG:2% Cr^{3+} , 1% Yb^{3+} was cut using a diamond saw and polished for absorption measurements. For luminescence experiments, selected crystals of the various concentrations were directly used.

B. Spectroscopic measurements

Absorption spectra of a YGG:2% Cr^{3+} , 1% Yb^{3+} crystal of 2.70 mm thickness mounted in a copper cell were mea-

sured on a Cary 5E (Varian) spectrometer. Sample cooling was achieved using a closed-cycle cryostat (Air Products). Continuous-wave upconversion luminescence spectra were excited by an Ar^+ -ion laser (Spectra Physics 2060-10 SA) pumped tunable Ti:sapphire laser (Spectra Physics 3900S). The emission was dispersed by a 0.85-m double monochromator (Spex 1402) using 500-nm blazed 1200 grooves/mm gratings and detected by a cooled photomultiplier (Hamamatsu 3310-01) and recorded with a photon-counting system (Stanford Research SR 400). Continuous-wave downconversion luminescence spectra were excited with the Ti:sapphire laser or the 457.9-nm line of the Ar^+ -ion laser and detected as described above. In all the measurements the laser beam was focused on the crystal with a lens of focal length $f=53$ mm. All the spectra were corrected for the sensitivity of the monochromator and detection system and the refractive index of air (vacuum correction). They are represented as photon counts versus wave numbers. For excitation spectra, the Ti:sapphire laser was scanned using an inchworm controller (Burleigh PZ-501) to drive a birefringent filter, and the wavelength was monitored with a wavemeter (Burleigh WA2100). All excitation scans were corrected for the power dependence of the Ti:sapphire laser source over the tuning range. For two-color experiments two Ti:sapphire lasers were used as excitation sources.

For pulsed upconversion and Yb^{3+} downconversion excitation experiments the output of a Nd:YAG (yttrium aluminum garnet) laser (Quanta Ray DCR 3) pumped dye laser (Lambda Physik FL3002, Pyridine 1) was Raman shifted (Quanta Ray, RS-1, H_2 , 340 psi). For time-resolved Cr^{3+} downconversion the output of the dye laser was directly used. The sample luminescence was dispersed by a 0.75-m single monochromator (Spex 1702) equipped with a 750-nm blazed 600 grooves/mm grating and detected by a cooled photomultiplier (Hamamatsu 3310-01) and recorded with a multichannel scaler (Stanford Research SR430). Sample cooling was achieved using a quartz He flow tube for luminescence measurements.

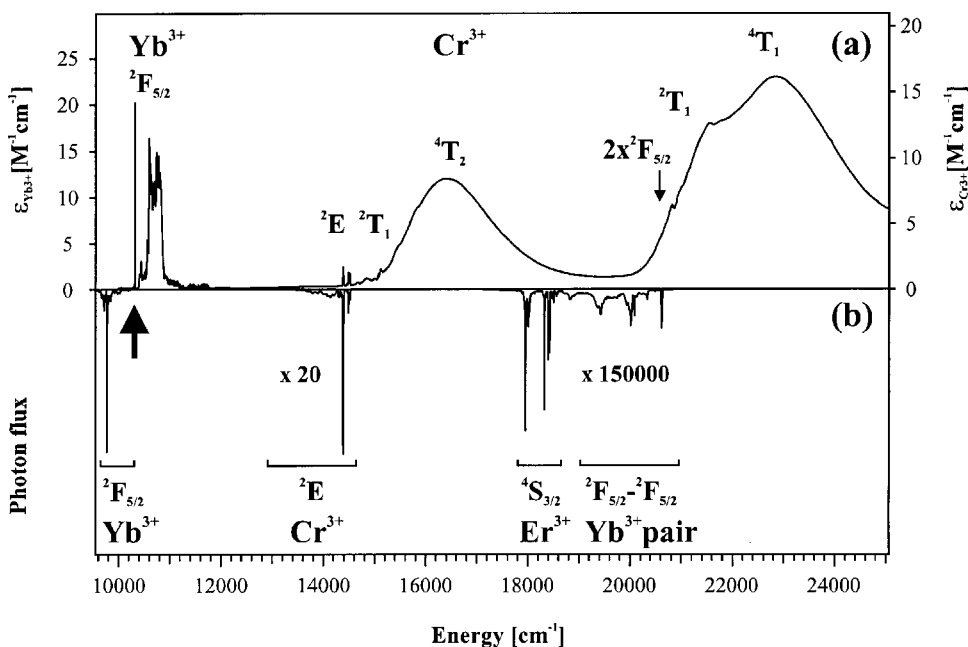


FIG. 1. (a) shows the relevant part of the absorption spectrum of YGG: 2% Cr^{3+} , 1% Yb^{3+} at 13 K. The y axis on the left and the right side give the extinction coefficients for Yb^{3+} and Cr^{3+} , respectively. The excited states of Cr^{3+} and Yb^{3+} are assigned. (b) shows the 15 K upconversion luminescence spectra after laser excitation at $10\,314\text{ cm}^{-1}$ (indicated by the arrow) of YGG: 2% Cr^{3+} , 1% Yb^{3+} . The laser power was 150 mW with a focusing lens of 53 mm. The emitting states are assigned. The Cr^{3+} and Yb^{3+} -pair/ Er^{3+} emissions are blown up by factors of 20 and 150 000, respectively.

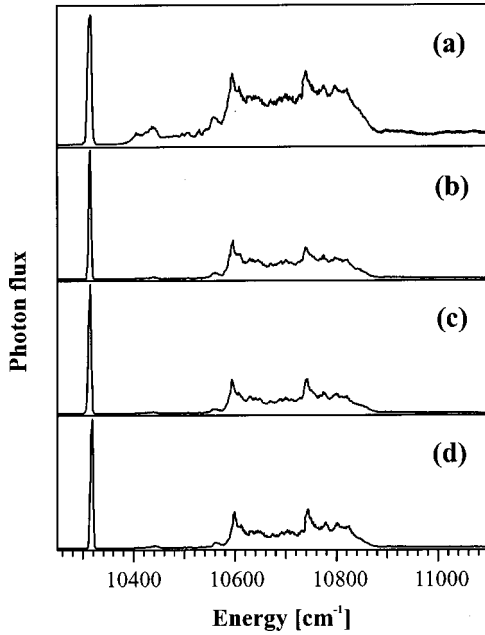


FIG. 2. Comparison of excitation spectra of YGG: 2% Cr^{3+} , 1% Yb^{3+} at 15 K in the region of the ${}^2F_{7/2} \rightarrow {}^2F_{5/2}$ transition of Yb^{3+} . (a), (b), and (c) are the excitation scans monitoring the NIR Yb^{3+} (at 9770 cm^{-1}), the red Cr^{3+} (at 14388 cm^{-1}) and the green Yb^{3+} -pair luminescence (20628 cm^{-1}) intensities, respectively. (d) shows the square of spectrum in (a).

III. RESULTS

The overview 13-K absorption and 15-K upconversion luminescence spectra of YGG:2% Cr^{3+} , 1% Yb^{3+} excited at 10314 cm^{-1} are depicted in Figs. 1(a) and 1(b), respectively. In the NIR between 10000 and 11000 cm^{-1} , the absorption is assigned to the ${}^2F_{7/2} \rightarrow {}^2F_{5/2}$ transitions of Yb^{3+} . The VIS spectral region consists of the typical absorption bands of Cr^{3+} in an octahedral oxo coordination. 150-mW laser excitation at 10314 cm^{-1} into the prominent absorption line (indicated by the arrow) at 15 K leads to $\text{Yb}^{3+} {}^2F_{5/2} \rightarrow {}^2F_{7/2}$ luminescence in the NIR. In addition, we observe a relatively intense red emission and very weak features in the green between 18000 and 21000 cm^{-1} . The number of emitted photons in the red (13000 – 14530 cm^{-1}) and green (18000 – 20640 cm^{-1}) spectral regions are 18 and 35000 times smaller, respectively, than for the ${}^2F_{5/2}$ NIR luminescence of Yb^{3+} (9500 – 10000 cm^{-1}). The upconversion efficiency, i.e., the fraction of emitted VIS photons, is thus 5.6% at 15 K for this excitation density. The red and green emissions are assigned to Cr^{3+} and Er^{3+} , Yb^{3+} , respectively. Below 200 mW at 15 K the red and green upconversion luminescence intensities excited at 10314 cm^{-1} show a quadratic dependence on the laser-excitation power, whereas the $\text{Yb}^{3+} {}^2F_{5/2} \rightarrow {}^2F_{7/2}$ luminescence has a linear dependence.

Figure 2 shows a comparison of excitation spectra of YGG:2% Cr^{3+} , 1% Yb^{3+} at 15 K. Figures 2(a), 2(b), and 2(c) are the excitation scans monitoring the NIR Yb^{3+} , the red Cr^{3+} , and the green Yb^{3+} -pair luminescence intensity, respectively. Figure 2(d) shows the square of the NIR Yb^{3+} excitation spectrum of Fig. 2(a).

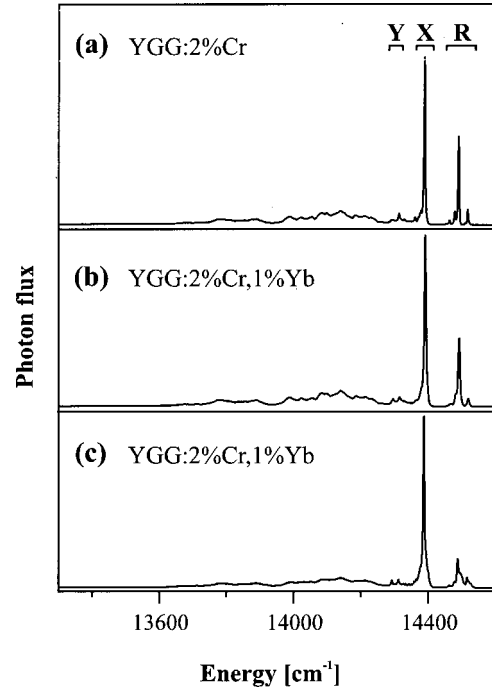


FIG. 3. (a) and (b) show the 15 K luminescence spectra of YGG: 2% Cr^{3+} and YGG: 2% Cr^{3+} , 1% Yb^{3+} , respectively, after 21839 cm^{-1} laser excitation. (c) shows the 15 K upconversion luminescence spectrum of YGG: 2% Cr^{3+} , 1% Yb^{3+} after 10314 cm^{-1} laser excitation.

Figure 3 compares the 15-K downconversion luminescence spectra of YGG:2% Cr^{3+} [Fig. 3(a)] and YGG:2% Cr^{3+} , 1% Yb^{3+} [Fig. 3(b)], both excited at 21839 cm^{-1} , with the 15-K red-upconversion luminescence spectrum of YGG:2% Cr^{3+} , 1% Yb^{3+} excited at 10314 cm^{-1} Fig. 3(c). The three spectra show a close analogy: The 14290 – 14550 cm^{-1} region that is dominated by sharp lines is followed by a broader, slightly structured band on the lower energy side. The relative contribution of the sharp lines to the total luminescence intensity of this spectral region is enhanced by a factor of 2.4 in the spectrum excited at 10314 cm^{-1} .

Figure 4 shows the red-upconverted luminescence spectra of YGG:2% Cr^{3+} , 1% Yb^{3+} after 10314-cm^{-1} excitation with 150 mW laser power at various temperatures. The spectra above 50 K are blown up by the scaling factors given on the right-hand side. The integrated photon flux decreases rapidly with increasing temperature above 50 K. Above 100-K the broadband luminescence, extending from 12000 to 15500 cm^{-1} , replaces the sharp features observed at low temperatures.

Figure 5 shows the 15-K upconversion-luminescence spectra in the region 14250 – 14550 cm^{-1} of three samples with different Cr^{3+} concentrations upon 150-mW laser excitation at 10314 cm^{-1} . Increasing the Cr^{3+} concentration leads to a small decrease of the overall red-upconversion efficiency: At 15 K the efficiencies are 5.6%, 2.3%, and 1.7% in the garnets YGG:2% Cr^{3+} , 1% Yb^{3+} , YGG:5% Cr^{3+} , 1% Yb^{3+} and YGG:14% Cr^{3+} , 1% Yb^{3+} , respectively. All three samples show three similar groups of lines separated by roughly 100 cm^{-1} , see the Y, X, and R systems in Fig. 5.

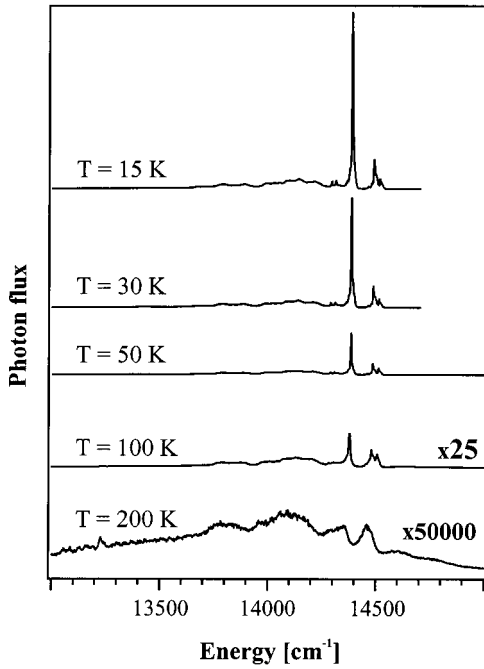


FIG. 4. Temperature dependence of the upconversion luminescence spectrum of YGG: 2% Cr^{3+} , 1% Yb^{3+} in the region 13 000–15 000 cm^{-1} after 10 314 cm^{-1} laser excitation. The temperatures are indicated on the left side. Note the scaling factors on the right side.

With increasing Cr^{3+} concentration, the intensity shifts from the R to the X to the Y system. Site-selective spectroscopy in YGG:2% Cr^{3+} , 1% Yb^{3+} in the region 14 250–14 550 cm^{-1} at 15 K revealed two different pairs of corresponding R lines. In Fig. 5 they are labeled R_1 (14 488 cm^{-1}), R_2 (14 516 cm^{-1}), and R'_1 (14 497 cm^{-1}), R'_2 (14 524 cm^{-1}), separated by 28 and 27 cm^{-1} , respectively. In the X and Y systems, no corresponding pairs of lines were observed.

The curves (a) and (b) in Fig. 6 show the measured time dependence of the 15-K red downconversion (excited at 14 641 cm^{-1}) and upconversion (excited at 10 315 cm^{-1}) luminescence intensities, respectively, of YGG:2% Cr^{3+} , 1% Yb^{3+} after a 10-ns excitation pulse detected at 14 388 cm^{-1} (X line). The inset shows the upconversion transient with a better time resolution. The solid lines represent fits to the experimental data and will be discussed in Sec. IV C 2.

In Fig. 7 the diamond markers (\blacklozenge) represent the integrated photon ratio (in a logarithmic representation) of the VIS (red) to NIR emission after 10 314- cm^{-1} excitation as a function of $1/T$. The circle markers (\bullet) represent the integrated photon ratio (in a logarithmic representation) of the NIR to VIS (red) emission after 21 839- cm^{-1} excitation as a function of $1/T$. The solid lines represent fits to the experimental data and will be discussed in Sec. IV D.

IV. DISCUSSION

A. Substitution of Yb^{3+} in YGG and single ion spectroscopy

Yb^{3+} has a $4f^{13}$ electron configuration giving rise to the ground and excited multiplets $^2F_{7/2}$ and $^2F_{5/2}$, respectively.

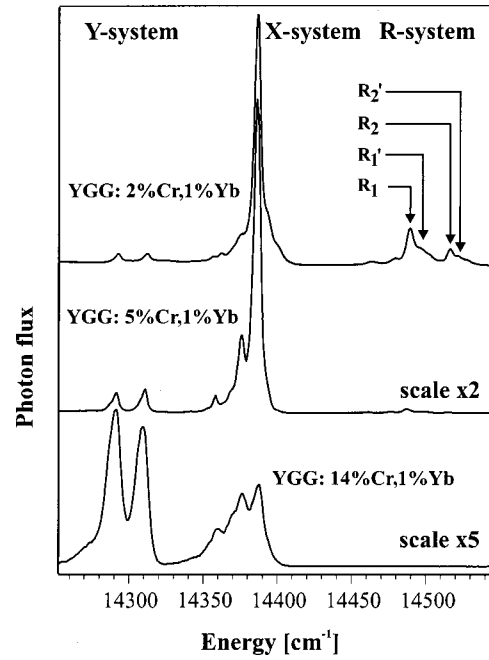


FIG. 5. The top, middle, and bottom parts show the upconversion luminescence spectra of YGG: 2% Cr^{3+} , 1% Yb^{3+} , YGG: 5% Cr^{3+} , 1% Yb^{3+} , and YGG: 14% Cr^{3+} , 1% Yb^{3+} , respectively, upon 10 314 cm^{-1} excitation at 15 K.

The two multiplets are separated by roughly 10 000 cm^{-1} . Above 10 000 cm^{-1} Yb^{3+} is transparent throughout the NIR and VIS. In an oxide environment the first allowed transitions are the ligand-to-metal charge transfer or $f-d$ transitions on the Yb^{3+} . They fall outside the range of the overview absorption spectrum of YGG:2% Cr^{3+} , 1% Yb^{3+} shown in Fig. 1.¹⁶ In Yb^{3+} compounds the electronic $f-f$ transitions between the $^2F_{7/2}$ and $^2F_{5/2}$ multiplets are usually

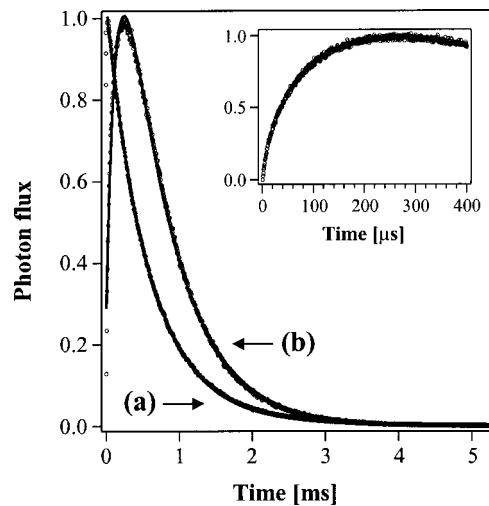


FIG. 6. 15 K time evolution of YGG: 2% Cr^{3+} , 1% Yb^{3+} luminescence following 10 ns pulsed excitation. (a) and (b) show the X -line intensity for 14 641 and 10 314 cm^{-1} excitation, respectively. The inset shows the rise of (a) with a better time resolution. The solid lines are least-squares fits of Eq. (1) to the experimental data as explained in the text in Sec. IV C 2.

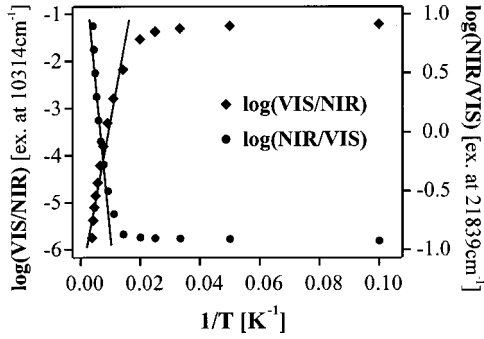


FIG. 7. The diamond markers (◆) represent the integrated photon ratio of the red to NIR emission (in log representation) after 10314 cm^{-1} excitation as a function of $1/T$. The circle markers (●) represent the integrated photon ratio of the NIR to red emission (in log representation) after 21839 cm^{-1} excitation as a function of $1/T$. The solid lines are least square fits of Eq. (2) to the experimental data below 70 K as described in Sec. IV D.

accompanied by remarkably intense vibronic sidebands. Due to the large energy gap between ${}^2F_{7/2}$ and ${}^2F_{5/2}$ of roughly 10000-cm^{-1} multiphonon relaxation is not important in Yb^{3+} -doped ionic compounds and ${}^2F_{5/2}$ luminescence is commonly observed. These properties make Yb^{3+} an excellent upconversion sensitizer for ions such as Tm^{3+} ,¹⁷ Er^{3+} ,¹⁸ Ho^{3+} ,¹⁹ and Pr^{3+} .²⁰

The absorption and luminescence spectra of YGG:1% Yb^{3+} have been analyzed in Ref. 21, and we only give a brief summary here. In YGG, Yb^{3+} replaces Y^{3+} on a site of D_2 point symmetry. In this low-symmetry environment ${}^2F_{7/2}$ and ${}^2F_{5/2}$ are split into four and three crystal-field levels labeled $0, 1, 2, 3$ and $0', 1', 2'$, respectively. The absorption, luminescence, and excitation spectra of YGG:2% Cr^{3+} , 1% Yb^{3+} at 15 K in Figs. 1 and 2 show the transitions between these levels around 10000 cm^{-1} . The spectra are complicated by the presence of intense vibronic sidebands, which obscure most of the electronic transitions and make an assignment very difficult. The $0 \leftrightarrow 0'$ transition at 10314 cm^{-1} is the only well-separated, sharp zero-phonon line typical of lanthanide f - f transitions. Its intensity is drastically reduced in the 15-K luminescence spectrum due to reabsorption, see Fig. 1. The absorption and luminescence spectra of Yb^{3+} are similar to those reported in Ref. 21, which shows that the presence of Cr^{3+} does not significantly affect the Yb^{3+} electronic structure. In YGG:2% Cr^{3+} , 1% Yb^{3+} and YGG:1% Yb^{3+} the decay of the Yb^{3+} ${}^2F_{5/2}$ luminescence intensity at 15 K is single exponential with lifetimes of $485\text{ }\mu\text{s}$ and $880\text{ }\mu\text{s}$, respectively, after excitation at 10315 cm^{-1} . The lifetime of the YGG:1% Yb^{3+} sample is similar to the value of 1.1 ms observed for YAG: Yb^{3+} (Ref. 22) while codoping with Cr^{3+} leads to a significant reduction of the Yb^{3+} ${}^2F_{5/2}$ lifetime.

B. Substitution of Cr^{3+} in YGG and single-ion spectroscopy

The optical spectroscopy of Cr^{3+} has been studied in numerous materials. In crystals, glasses, and molecular complexes Cr^{3+} exclusively adopts an octahedral ligand coordination that is usually slightly distorted. The absorption (and

luminescence) of Cr^{3+} -doped YGG has been reported in the literature.^{23–27} Here we focus on those aspects that are relevant for the upconversion process. In YGG, Cr^{3+} replaces the octahedrally coordinated Ga^{3+} ions with S_6 -site symmetry. Since Cr^{3+} has the $3d^3$ electron configuration, the ground state is 4A_2 (O notation). The nature of the first excited state depends on the crystal-field strength and is either the 2E or the 4T_2 state.²⁶ The ${}^4A_2 \rightarrow {}^2E$ and the closely lying ${}^4A_2 \rightarrow {}^2T_1$ transitions take place within the t_2^3 electron configuration. As a consequence, these so-called spin-flip transitions have small Huang-Rhys parameters and appear as weak and sharp lines in the spectrum. On the other hand, the spin-allowed ${}^4A_2 \rightarrow {}^4T_2$ transition appears as a more intense and broad band with a large Huang-Rhys parameter.²⁸ The absorption spectrum in Fig. 1(a) shows that in YGG:2% Cr^{3+} , 1% Yb^{3+} the ${}^4A_2 \rightarrow {}^2E$, 2T_1 lines appear just below the onset of the broad ${}^4A_2 \rightarrow {}^4T_2$ band centered at about 16400 cm^{-1} . Above 20000 cm^{-1} we identify the second broad spin-allowed d - d band ${}^4A_2 \rightarrow {}^4T_1$, centered at about 22800 cm^{-1} and the sharp features around 21200 cm^{-1} corresponding to ${}^4A_2 \rightarrow {}^2T_2$ spin-flip transitions. From these band positions we determined $Dq = 1640\text{ cm}^{-1}$, $B = 640\text{ cm}^{-1}$, $C = 3240\text{ cm}^{-1}$, which are in good agreement with the values in Ref. 25.

In the S_6 site occupied by Cr^{3+} the octahedral coordination is trigonally distorted along the diagonals of the cubic unit cell. The 2E state, which is the emitting state and thus of major interest in this study, is split by the combined action of spin-orbit coupling and the trigonal ligand field into the spinor components $\bar{2}A$ and \bar{E} .²⁸ Transitions to and from these components are observed in the absorption and luminescence spectra. In ruby the 2E components are known as R lines. In the low-temperature absorption spectrum of YGG:2% Cr^{3+} , 1% Yb^{3+} in Fig. 1 as well as in the luminescence spectra of YGG:2% Cr^{3+} , 1% Yb^{3+} and YGG:2% Cr^{3+} in Fig. 3, we observe more than the two expected sharp R_1 and R_2 lines in the 14250 – 14530 cm^{-1} region. These lines are labeled with $R, X,$ and Y in Fig. 3 and occur at the same energetic positions in absorption and luminescence. They are assigned to 2E electronic origins of different Cr^{3+} sites. Using site-selective spectroscopy we found that even the R system contains more than one Cr^{3+} site. We identified two R -line pairs with 2E splittings of 28 and 27 cm^{-1} labeled R_1/R_2 and R'_1/R'_2 , respectively, in Fig. 5. These splittings are in good agreement with the R -line splitting of 27 cm^{-1} reported for YGG: Cr^{3+} in Ref. 23. We were unable to determine the 2E splitting in the other lines of the $R, X,$ and Y system. The sharp origin lines are followed by the expected weakly structured phonon sidebands, see Fig. 3.

Multisite effects in the garnet lattices have been studied in detail and were attributed to cation inversion.^{24,27,29,30} These effects lead to energetic shifts of the R lines on the order of 40 cm^{-1} , which is significantly smaller than the 250 cm^{-1} spread of the $R, X,$ and Y systems in Fig. 5. Exchange effects are not the origin for this splitting either, as Cr^{3+} occupies isolated octahedrally coordinated sites in garnets, thus leading to small exchange splittings of the order of the inhomogeneously broadened linewidths.³¹

As no Y and X systems were described for YGG:Cr³⁺ in the literature, we attribute the occurrence of these additional lines in the title compound to our synthesis method. The additional lines are observed in all the Cr³⁺-doped YGG crystals grown from a Bi₂O₃ flux, independent of Yb³⁺ and Cr³⁺ concentration, see Figs. 3 and 5. The importance of the X and Y sites strongly increases with Cr³⁺ concentration. ICP analysis showed that our crystals contain about 1–2 % of the flux ion Bi³⁺, which most likely replaces Y³⁺ ions. Due to the ionic radius of Bi³⁺ (1.17 Å), which is much larger than that of Y³⁺ (1.019 Å), a big distortion of the lattice around Bi³⁺ is expected.³² This could in turn lead to distorted Cr³⁺ sites in the neighborhood of Bi³⁺ and thus give rise to the X and Y bands. As shown in Fig. 3, the occurrence of the X and Y lines is independent of the presence of Yb³⁺.

C. Upconversion

Figure 1 shows that at 15-K Cr³⁺ upconversion luminescence is induced quite efficiently upon excitation around 10 000 cm⁻¹ into ²F_{5/2} of Yb³⁺. This new mode of inducing ²E→⁴A₂ Cr³⁺ luminescence after NIR Yb³⁺ excitation is unexpected and remarkable. There are many upconversion phenomena reported in lanthanide-doped crystals and glasses. Since the f electrons are well shielded from their ligand-field environment, the electron-phonon coupling is small and therefore more than one metastable excited state with a sufficiently long lifetime is available in most lanthanide systems. In contrast, the d electrons of transition metal ions are less well shielded, the electron-phonon coupling is stronger, and nonradiative multiphonon relaxation processes are much more competitive. Thus, it is not surprising that multi-excited-state luminescence and upconversion processes are very rare in transition-metal ion systems. Some examples of upconversion phenomena are reported on transition-metal ion systems to date: Ti²⁺,⁴ Ni²⁺,⁵ Mo³⁺,⁶ Re⁴⁺,⁷ and Os⁴⁺.⁸ The combination of transition-metal (TM) and rare-earth (RE) metal ions in the same crystal is an appealing approach to explore new cooperative processes such as upconversion. The possibility to tune the properties of a transition-metal ion by chemical and structural variation together with the relative inertness of the rare-earth ions toward such variation is promising. Very recently, we reported on Yb³⁺-to-Mn²⁺ upconversion processes in RbMnCl₃:Yb³⁺,^{9,10} CsMnCl₃:Yb³⁺,^{10,11} and CsMnBr₃:Yb³⁺.¹² These studies yielded some very surprising and intriguing results, and at least two different upconversion mechanisms were found to be at work. Since Yb³⁺ is transparent above 11 200 cm⁻¹ throughout the NIR and VIS spectral region it is an excellent partner for such mixed TM/RE systems. The title system YGG:2% Cr³⁺, 1% Yb³⁺ is the first one to exhibit VIS Cr³⁺ emission excited by direct NIR upconversion via Yb³⁺. The mode of Cr³⁺ ²E→⁴A₂ luminescence excitation by an upconversion process in which both the Yb³⁺ and the Cr³⁺ ions are directly involved is new.^{33,34} Our process is distinctly different in that both Yb³⁺ and Cr³⁺ are active partners in the upconversion process.

Beside the strong red luminescence we observe a very weak green luminescence after NIR excitation of YGG:2%

Cr³⁺, 1% Yb³⁺ at 15 K. This is not our main interest in this study. Nevertheless, this green upconversion luminescence with all its fine structure can be completely understood.

1. Green upconversion luminescence

The very weak green upconversion luminescence observed at 15 K between 17 800 and 20 630 cm⁻¹ (see Fig. 1) can be divided into two parts on the basis of its fine structure. The region 17 800–18 700 cm⁻¹ is built of very sharp and closely spaced lines whereas the region 18 700–20 630 cm⁻¹ shows much broader features.

The upconverted luminescence in the region 17 800–18 700 cm⁻¹ is identified as the ⁴S_{3/2}→⁴I_{15/2} transition of Er³⁺ by comparison with Ref. 35. This Er³⁺ impurity that was likely introduced with the Yb₂O₃ starting material, could be detected in our crystals by the ICP method, with an upper limit of 0.001% in all the samples. The excitation spectrum of the ⁴S_{3/2} upconversion luminescence follows the ²F_{7/2}→²F_{5/2} absorption spectrum of Yb³⁺, which identifies Yb³⁺ as the sensitizer for this upconversion process. Yb³⁺ sensitized Er³⁺ upconversion is a well-established and very efficient process in oxide and halide crystals and glasses codoped with Yb³⁺ and Er³⁺. The Yb³⁺ ²F_{5/2} excitation is transferred to Er³⁺ ⁴I_{11/2}, followed by the upconversion process to ⁴F_{7/2} and then multiphonon relaxation to ⁴S_{3/2}. At a given laser power the intensity ratio of the Er³⁺ ⁴S_{3/2} emission to the Yb³⁺ ²F_{5/2} emission in the NIR is the same for YGG:2% Cr³⁺, 1% Yb³⁺ and YGG:1% Yb³⁺. From this observation we can unambiguously rule out that the ²E→⁴A₂ emission of Cr³⁺ in YGG:2% Cr³⁺, 1% Yb³⁺ is excited via an Yb³⁺/Er³⁺ upconversion process.

For energy reasons the green upconversion luminescence in the region 18 700–20 630 cm⁻¹ is identified as cooperative Yb³⁺-pair luminescence.^{36,37} The upconversion excitation spectrum of this luminescence shown in Fig. 2(c) is very similar to the excitation spectrum of the red Cr³⁺ ²E→⁴A₂ upconversion luminescence shown in Fig. 2(b). It reflects the energy and intensity distributions of the squared absorption spectrum shown in Fig. 2(d). This is a very nice illustration of the quadratic character of this upconversion excitation, which is also reflected in the quadratic power dependence of the upconversion-luminescence intensity.

The individual lines of this cooperative green luminescence can be assigned to (²F_{5/2}-²F_{5/2})→(²F_{7/2}-²F_{7/2}) transitions of Yb³⁺ dimers with energies corresponding to the sum of single-ion Yb³⁺ transitions. The intensity of this cooperative upconversion luminescence in YGG:2% Cr³⁺, 1% Yb³⁺ at 15 K is 20 000 times weaker than the ²E→⁴A₂ upconversion luminescence intensity of Cr³⁺.

2. Yb³⁺-to-Cr³⁺ upconversion

The quadratic dependence of the Cr³⁺ upconversion luminescence intensity on the power of the NIR laser excitation at 10 314 cm⁻¹ is evidence for a two-photon process. The upconversion excitation spectrum of the red Cr³⁺ ²E→⁴A₂ upconverted luminescence in Fig. 2(b) is very similar in terms of energies and relative intensities to the squared

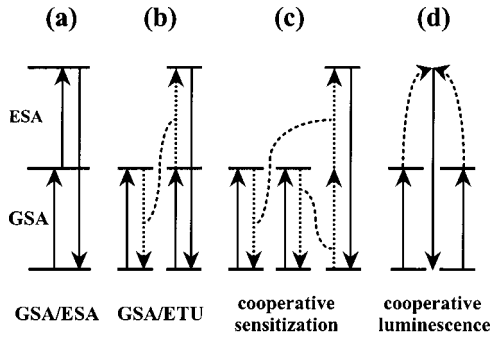


FIG. 8. Schematic representation of the four most relevant photon upconversion mechanisms. The full arrows represent radiative transitions and dashed lines and arrows represent nonradiative processes.

NIR excitation spectrum in Fig. 2(d). This demonstrates that two $\text{Yb}^{3+} {}^2F_{7/2} \rightarrow {}^2F_{5/2}$ excitations are involved in the upconversion process.

The four potentially most relevant UC mechanisms for our situation are schematically depicted in Fig. 8. A ground-state absorption (GSA) step to the intermediate state followed by an excited-state absorption (ESA) step to the upper state is shown in Fig. 8(a).³⁸ The process (b) denoted GSA/ETU involves an energy transfer step between two ions that are in close proximity and both excited to their intermediate states.¹⁸ The process (c) in Fig. 8 is the least established among the four. It has been postulated to account for the VIS emission after NIR absorption in Tb^{3+} - and Yb^{3+} -codoped BaF_2 and YF_3 . It is a cooperative sensitization process, involving two excited donor ions and an acceptor ion in close proximity.³⁹ In the cooperative upconversion process (d) two ions in close proximity excited to their intermediate states combine their energy to emit a photon at twice the energy. The single ions do not have stationary states at the emission energy.⁵⁶ The green Yb^{3+} luminescence discussed in Sec. IV C 1 is the most prominent example of such a mechanism.

GSA/ESA and GSA/ETU are the best established mechanisms in lanthanide-doped materials. The GSA/ESA sequence usually takes place on a single ion. This can definitely be ruled out in the present situation, because it is established that both Yb^{3+} and Cr^{3+} are involved in the process. However, a modified version of GSA/ESA has recently been invoked to account for the observation of VIS Mn^{2+} emission after NIR absorption in Yb^{3+} -doped RbMnCl_3 and CsMnBr_3 . Instead of a single ion an exchange-coupled Yb^{3+} - Mn^{2+} dimer was considered as the relevant chromophoric unit. A similar mechanism has to be considered here. Of the two mechanisms involving an energy-transfer step, GSA/ETU [Fig. 9(b)] and cooperative sensitization [Fig. 9(d)], only the latter is a candidate in the present situation, because Cr^{3+} does not have any excited states below ${}^2E \rightarrow {}^4A_2$. We thus have to discuss the modified version of GSA/ESA and the cooperative-sensitization mechanisms.

The time evolution of the upconverted luminescence intensity after a short excitation pulse contains important information on the upconversion mechanism. The experimental

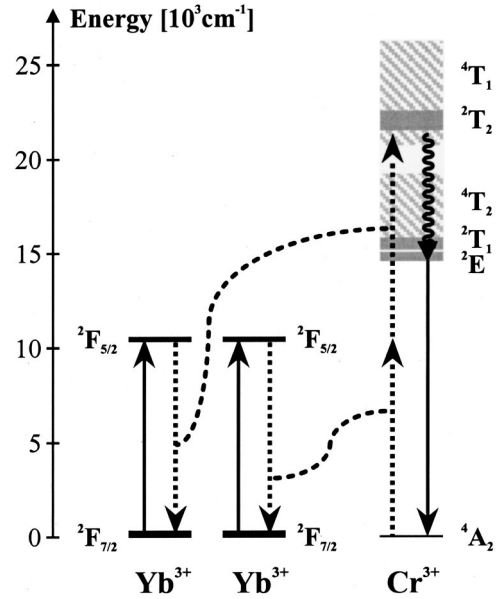


FIG. 9. Simplified energy level scheme with the relevant processes in the upconversion process: Straight up, dashed, curly and straight down arrows represent excitation, nonradiative energy transfer, nonradiative multiphonon relaxation and luminescence steps, respectively.

data on YGG:2% Cr^{3+} , 1% Yb^{3+} at 15 K are presented in Fig. 6 curve (b). In this experiment, the pulsed laser was tuned to the prominent Yb^{3+} absorption line at $10\,314\text{ cm}^{-1}$, and the Cr^{3+} upconversion luminescence transient was recorded at $14\,388\text{ cm}^{-1}$ (X system). The transient consists of an initial rise followed by a decay. The solid line in Fig. 6 curve (b) represents a least-squares fit of the empirical equation

$$I(t) = a_0 \exp(-t/\tau_{\text{decay}}) - a_1 \exp(-t/\tau_{\text{rise}}) \quad (1)$$

to the experimental data with a decay time $\tau_{\text{decay}} = 614\ \mu\text{s}$ and a rise time $\tau_{\text{rise}} = 145\ \mu\text{s}$. The inset to Fig. 6 shows that the rise starts at zero intensity immediately after the laser pulse. The 15-K decay transient of the ${}^2E \rightarrow {}^4A_2$ downconversion luminescence after direct Cr^{3+} excitation at $14\,641\text{ cm}^{-1}$ is depicted in Fig. 6 curve (a). It is essentially a single-exponential decay curve with a very weak rise part before $t = 30\ \mu\text{s}$. Despite this initial rise a single-exponential function was fitted to the experimental data, see the solid line in transient Fig. 6(a). We thus obtain a decay time $\tau_{\text{decay}} = 611\ \mu\text{s}$. This decay time compares well with the decay part of the upconversion transient in Fig. 6(b). A similar decay time $\tau_{\text{decay}} = 590\ \mu\text{s}$ was determined for the X system in YGG:2% Cr^{3+} . This decay time is shorter than the $\tau = 2.4\text{ ms}$ reported for the $\text{Cr}^{3+} {}^2E \rightarrow {}^4A_2$ luminescence in YGG:2% Cr^{3+} in Ref. 40. We attribute this shortening to the presence of the Bi^{3+} ions in the neighborhood of the X -type Cr^{3+} ions in our garnets.

The upconversion luminescence transient clearly indicates the presence of a slow step in the sequence of the processes that finally leads to ${}^2E \rightarrow {}^4A_2$ upconversion luminescence. This must be an energy transfer step. The situation is com-

plicated by the presence of energy transfer processes between the various Cr^{3+} sites discussed in Sec. IV B. Therefore, it is not *a priori* clear whether this slow step belongs to the upconversion process itself or to an energy transfer among the Cr^{3+} ions of different sites after the upconversion process. We attribute the very weak and short (Fig. 6) rise parts observed in the decay transients of the X line after direct Cr^{3+} excitation to the energy transfer between the various Cr^{3+} sites. This rise is one order of magnitude shorter than the rise time of 145 μs in the upconversion luminescence transient. This is a strong indication, although not an unambiguous proof, that the slow step in the sequence of processes leading to Cr^{3+} upconversion luminescence is the upconversion process itself. This rules out a GSA/ESA mechanism and is a first indication for the cooperative sensitization process.

Further strong evidence against a GSA/ESA sequence is provided by the results of the two-color excitation experiments. A hypothetical sequence of GSA/ESA steps in a one-color experiment with 10 314 cm^{-1} excitation energy would hit the Cr^{3+} in the foot of the ${}^4A_2 \rightarrow {}^4T_1$ absorption at 20 628 cm^{-1} , as indicated by the arrow in Fig. 1(a). We performed the following two-color experiment at 15 K: A first very weak laser of typically 2 mW output power was tuned to the Yb^{3+} GSA at 10 314 cm^{-1} . This produced a very weak upconversion luminescence in the red. A second intense laser of typically 300 mW output power, tuned to the $\text{Yb}^{3+} \rightarrow \text{Cr}^{3+}$ ESA at 12 500 cm^{-1} and thus hitting the 4T_1 band at 22 814 cm^{-1} , close to the absorption maximum, was then added. The GSA cross section is negligible at this wavelength, but the ESA cross section is certainly much bigger than at 10 314 cm^{-1} . The second laser did not enhance the upconversion luminescence intensity and thus we definitely rule out a GSA/ESA sequence.

Both the observed rise in the upconversion transients and the results of the two-color excitation experiments point towards the cooperative sensitization mechanism in Fig. 8(c). This mechanism is fully consistent with the similarity of the upconversion excitation spectrum of the red $\text{Cr}^{3+} {}^2E \rightarrow {}^4A_2$ upconverted luminescence and the squared NIR excitation spectrum of the $\text{Yb}^{3+} {}^2F_{7/2} \rightarrow {}^2F_{5/2}$ luminescence in Figs. 2(b) and 2(d), respectively. Figure 9 shows the relevant steps of this mechanism for YGG:2% Cr^{3+} , 1% Yb^{3+} . A prerequisite for such a mechanism to occur is either to have the Yb^{3+} donor ions arranged as dimers in the crystal or a high mobility of the Yb^{3+} excitation energy in the lattice. The garnets do not favor dimers of Yb^{3+} ions, we assume a statistical distribution among the Y^{3+} sites. We, therefore, attribute the high upconversion efficiency of 6% at 10 K to the high mobility of the $\text{Yb}^{3+} {}^2F_{5/2}$ excitation energy. Energy migration of the ${}^2F_{5/2}$ excitation among the Yb^{3+} ions has been reported for GGG:5% Yb^{3+} .⁴¹ Energy migration takes place at a doping level of 1% Er^{3+} in $\text{Cs}_3\text{Lu}_2\text{Br}_9$:1% Er^{3+} (Ref. 42) and is noticeable in YF_3 : Yb^{3+} , Ho^{3+} doped with 0.3% Yb^{3+} only.¹⁸ It is thus not unreasonable to assume a mobility of the ${}^2F_{5/2}$ excitation in YGG:2% Cr^{3+} , 1% Yb^{3+} studied here. Once two Yb^{3+} excitations are close to a Cr^{3+} ion, a resonant process in which two excited Yb^{3+} ions simultaneously transfer their excitation energy to the Cr^{3+}

becomes possible, since there is a small spectral overlap between twice the $\text{Yb}^{3+} {}^2F_{5/2} \rightarrow {}^2F_{7/2}$ emission and the $\text{Cr}^{3+} {}^4A_2 \rightarrow {}^4T_1$ absorption.

This energy transfer step is followed by fast nonradiative multiphonon relaxation to 2E , which is the emitting state, see Fig. 9.

D. Loss mechanisms

The data in Fig. 7 show that the ratio of VIS/NIR-emitted photons in YGG:2% Cr^{3+} , 1% Yb^{3+} after 10 314- cm^{-1} excitation (150 mW) drop almost linearly between 10 and 50 K from about 6–3%. Above 100 K the drop is exponential. At 250 K the VIS/NIR ratio has dropped by a factor of 10^{-5} compared to 10 K. The data in Fig. 7 are represented in the form of an Arrhenius plot, and an analysis of the high-temperature data (≥ 70 K) by the equation

$$\text{VIS/NIR} = A \exp(-\Delta E/kT) \quad (2)$$

yields an activation energy $\Delta E = (550 \pm 60) \text{ cm}^{-1}$, see the fit line through the diamond data in Fig. 7.

Figure 7 also contains the NIR/VIS photon ratio after blue 21 839- cm^{-1} excitation into 4T_1 of Cr^{3+} in a similar Arrhenius representation. This ratio is roughly constant at NIR/VIS=0.1 between 10 and 50 K, and above 100 K it increases exponentially with T . Applying Eq. (2) yields an activation energy $\Delta E = (460 \pm 50) \text{ cm}^{-1}$ (see the fit in Fig. 7). Within experimental accuracy this is the same value as obtained above for the VIS/NIR ratio in upconversion excitation. This immediately suggests that the thermal activation is due to the same process in both experiments.

It is obviously a process that transfers the excitation energy from Cr^{3+} to Yb^{3+} . Figure 4 contains the key to understanding it. At 15 K the Cr^{3+} luminescence is sharp lined and thus clearly assigned to ${}^2E \rightarrow {}^4A_2$. At temperatures of 100 K and higher the shape changes to broadband, and the assignment to ${}^4A_2 \rightarrow {}^4T_2$ is straightforward. The 4T_2 excited state is thermally populated in this temperature range, suggesting that this 4T_2 population may be responsible for the observed thermally activated excitation transfer from ${}^2E/{}^4T_2$ on Cr^{3+} to ${}^2F_{5/2}$ on Yb^{3+} . We determined an activation energy of about $\Delta E = (550 \pm 60) \text{ cm}^{-1}$ for this transfer. This compares very favorably with the energy difference of 650 cm^{-1} between the 4T_2 and 2E origins estimated from YGG: Cr^{3+} spectroscopy.⁴³

We conclude that $\text{Cr}^{3+} {}^4T_2$ to $\text{Yb}^{3+} {}^2F_{5/2}$ transfer is intrinsically more efficient by around seven orders of magnitude than $\text{Cr}^{3+} {}^2E$ to $\text{Yb}^{3+} {}^2F_{5/2}$ transfer, which determines the behavior below 50 K. We use the Yb^{3+} - Cr^{3+} dimer picture shown in Fig. 10 to interpret this. The crucial step is a multiphonon relaxation within this dimer. The relevant states in Fig. 10 have double labels and are plotted against a single configurational coordinate Q . Q represents the distortion coordinates of the 4T_2 excited state of Cr^{3+} . All the other states involved are essentially undistorted. We are interested in the ratio of the two multiphonon relaxation processes represented by bold and faint curly arrows in Fig. 10.

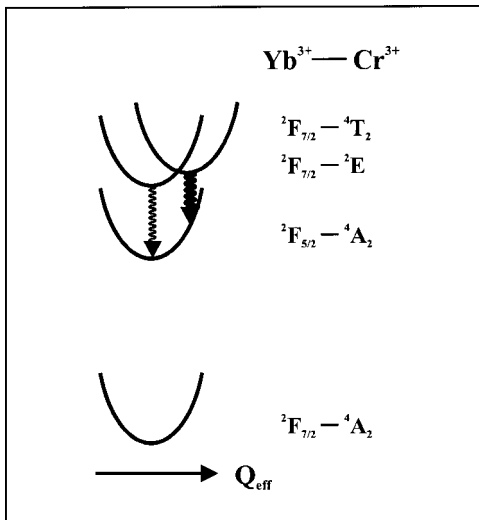


FIG. 10. Single-configurational coordinate picture of a Yb^{3+} - Cr^{3+} pair. The coordinate Q_{eff} is an effective distortion coordinate of the 4T_2 state of Cr^{3+} . The potentials carry double labels corresponding to the respective state of Yb^{3+} and Cr^{3+} . The faint and bold curly arrows represent the dominant relaxation processes at low and high temperatures, respectively.

Within the Condon approximation the nonradiative relaxation rate between two states $|b\rangle$ and $|a\rangle$ is proportional to a thermally averaged Franck-Condon (FC) factor within a single-configurational coordinate (SCC) model. At low temperatures this is given by:⁴⁴

$$FC_{T=0} = |\langle \chi_{a,p} \chi_{b,0} \rangle|^2 = \frac{e^{-S} S^p}{p!}, \quad (3)$$

where S is the Huang-Rhys factor, a measure of the distortion of the upper state $|b\rangle$ with respect to the lower state $|a\rangle$ along the coordinate Q , p is the reduced energy gap (in units of $\hbar\omega_Q$ between the $v=0$ levels of the $|a\rangle$ and $|b\rangle$). The 4T_2 state of Cr^{3+} is usually distorted along both the a_{1g} and e_g coordinates.^{45,46} This leads to an S_{eff} and a Q_{eff} comprising both distortions in our SCC model. From Figs. 1 and 4 we estimate the ${}^4A_2 \leftrightarrow {}^4T_2$ electronic origins at about 15000 cm^{-1} . Taking the average of the a_{1g} and e_g vibrational energies of the YGG lattice we get $\hbar\omega_{\text{eff}} \cong 500 \text{ cm}^{-1}$, and from the absorption and luminescence band shapes $S_{\text{eff}}({}^4T_2) \cong 2.5$. From the 2E luminescence band shapes $S_{\text{eff}}({}^2E) \cong 0.1$ should be an upper limit. The energy gap between the dimer states (${}^2F_{5/2-2}E$) and (${}^2F_{5/2-4}A_2$) is around 3500 cm^{-1} , corresponding to $p({}^2E) \cong 7$. 4T_2 lies about 650 cm^{-1} higher lead-

ing to $p({}^4T_2) \cong 8$. With these numbers we can now use Eq. (3) to estimate the relative importance of the two nonradiative relaxation processes in Fig. 10. The relaxation rate constant corresponding to the bold arrow is about 7–8 orders of magnitude bigger than that for the faint arrow. This is in very good agreement with the experimentally determined seven orders of magnitude.

At 15 K only the (${}^2F_{7/2-2}E$) \rightarrow (${}^2F_{5/2-4}A_2$) relaxation process is possible. Experimentally we find a NIR/VIS ratio of 10% after blue excitation at this temperature. So the faint arrow is just barely competitive with the radiative ${}^2E \rightarrow {}^4A_2$ process of Cr^{3+} . This is in good agreement with the 2E luminescence lifetimes determined at 15 K for YGG:2% Cr^{3+} and YGG:2% Cr^{3+} , 1% Yb^{3+} of 612 and 590 μs , respectively (see Sec. IV C).

V. CONCLUSIONS

We have identified and characterized a mode of exciting sharp Cr^{3+} ${}^2E \rightarrow {}^4A_2$ luminescence in YGG codoped with Cr^{3+} and Yb^{3+} . Excitation around 10314 cm^{-1} leads to relatively strong red Cr^{3+} luminescence at low temperatures. We propose a cooperative sensitization upconversion mechanism to account for this phenomenon. The characterization and description of the underlying processes is complicated by the presence of multisites in our crystals.

The described loss pathways are intrinsic for systems codoped with Cr^{3+} and Yb^{3+} . One possibility to reduce these is to strengthen the crystal field and thus increase the energy difference ΔE between 2E and 4T_2 . For this reason, we are planning to extend our studies to host materials such as YAG and YAlO_3 codoped with Cr^{3+} and Yb^{3+} . The situation is less favorable for systems with broadband Cr^{3+} ${}^4T_2 \rightarrow {}^4A_2$ luminescence, because in that case the nonradiative relaxation from Cr^{3+} 4T_2 to the Yb^{3+} ${}^2F_{5/2}$ multiplet is efficient and dominant down to the lowest temperatures.

Increasing the crystal field should also enhance the efficiency of the upconversion process. In the YGG lattice the spectral overlap between twice Yb^{3+} ${}^2F_{5/2} \rightarrow {}^2F_{7/2}$ emission and Cr^{3+} ${}^4A_2 \rightarrow {}^4T_1$ absorption is small and thus the efficiency of the energy transfer step in the upconversion process limited. At a higher crystal field the 4T_2 band would move to higher energy and thus create the necessary spectral overlap. We are presently exploring this avenue.

ACKNOWLEDGMENT

Financial support from the Swiss National Science Foundation is gratefully acknowledged.

*Corresponding author. FAX: +41 31 631 43 99. Email: hans-ulrich.guedel@iac.unibe.ch

¹M. F. Joubert, Opt. Mater. **11**, 181 (1999).

²E. Downing, L. Hesselink, J. Ralston, and R. Macfarlane, Science **273**, 1185 (1996).

³J. S. Chivian, W. E. Case, and D. D. Eden, Appl. Phys. Lett. **35**, 124 (1979).

⁴S. M. Jacobsen and H. U. Güdel, J. Lumin. **43**, 125 (1989).

⁵U. Oetliker, M. J. Riley, P. S. May, and H. U. Güdel, J. Lumin. **53**, 553 (1992).

⁶D. R. Gamelin and H. U. Güdel, J. Am. Chem. Soc. **120**, 12 143 (1998).

⁷D. R. Gamelin and H. U. Güdel, Inorg. Chem. **38**, 5154 (1999).

⁸M. Wermuth and H. U. Güdel, J. Am. Chem. Soc. **121**, 10 102 (1999).

⁹R. Valiente, O. S. Wenger, and H. U. Güdel, Phys. Rev. B **63**,

- 165102 (2001).
- ¹⁰R. Valiente, O. S. Wenger, and H. U. Güdel, *Chem. Phys. Lett.* **320**, 639 (2000).
- ¹¹R. Valiente, O. S. Wenger, and H. U. Güdel, *J. Chem. Phys.* (to be published).
- ¹²P. Gerner, O. S. Wenger, R. Valiente, and H. U. Güdel, *Inorg. Chem.* **40**, 4534 (2001).
- ¹³F. Eueler and J. A. Bruce, *Acta Crystallogr.* **19**, 971 (1965).
- ¹⁴S. Heer, M. Wermuth, K. Krämer, and H. U. Güdel, *Chem. Phys. Lett.* **334**, 293 (2001).
- ¹⁵B. M. Wanklyn, *J. Cryst. Growth* **54**, 610 (1981).
- ¹⁶P. Dorenbos, *J. Lumin.* **91**, 155 (2000).
- ¹⁷F. W. Ostermayer *et al.*, *Phys. Rev. B* **3**, 2698 (1971).
- ¹⁸M. F. Auzel, *C. R. Acad. Sci. Paris Ser. B* **262**, 1016 (1966).
- ¹⁹R. K. Watts and H. J. Richter, *Phys. Rev. B* **6**, 1584 (1972).
- ²⁰B. Jaquier *et al.*, *J. Lumin.* **60/61**, 175 (1997).
- ²¹R. A. Buchanan, K. A. Wickersheim, J. J. Pearson, and G. F. Herrmann, *Phys. Rev.* **159**, 245 (1967).
- ²²G. A. Bogomolova, D. N. Vylegzhanin, and A. A. Kaminskii, *Zh. Eksp. Teor. Fiz.* **69**, 860 (1975) [*Sov. Phys. JETP* **42**, 440 (1976)].
- ²³G. Burns, E. A. Geiss, B. A. Jenkins, and I. N. Marshall, *Phys. Rev.* **B139**, 1687 (1965).
- ²⁴M. Yamaga *et al.*, *J. Lumin.* **39**, 335 (1988).
- ²⁵K. P. O'Donell *et al.*, *J. Lumin.* **42**, 365 (1989).
- ²⁶M. Grinberg, *J. Lumin.* **54**, 369 (1993).
- ²⁷A. P. Vink, J. Meijerink, *J. Lumin.* **61**, 1717 (2000).
- ²⁸S. Sugano, Y. Tanabe, and H. Kamimura, *Multiplets of Transition Metal Ions in Crystals* (Academic, London, 1970).
- ²⁹A. Monteil, W. Nie, C. Madej, and G. Boulon, *Opt. Quantum Electron.* **22**, 247 (1990).
- ³⁰W. Nie, A. Monteil, and G. Boulon, Vol. 249 of *NATO Advanced Study Institute, Series B: Physics* (Adv. Nonradiative Processes Solids, 1991), p. 425.
- ³¹R. Wannemacher, and J. Heber, *J. Lumin.* **39**, 49 (1987).
- ³²R. D. Shanon, *Acta Crystallogr., Sect. A: Cryst. Phys., Diffr., Theor. Gen. Crystallogr.* **A32**, 751 (1976).
- ³³K. S. Lim, C. W. Lee, S. T. Kim, H. J. Seo, and C. D. Kim, *J. Lumin.* **87–89**, 1008 (2000).
- ³⁴R. Micheletti, P. Minguzzi, M. A. Noginov, and M. Tonelli, *J. Opt. Soc. Am. B* **11**, 2095 (1994). (There have been reports in the literature of Cr³⁺ emission after NIR excitation in Er³⁺ or Ho³⁺/Tm³⁺-codoped garnet crystals.^{33,34} However, according to Refs. 33 and 34 the upconversion takes place on the Er³⁺ or Ho³⁺/Tm³⁺ ions in these crystals, before the excitation is transferred to Cr³⁺.)
- ³⁵X. Chen, T. Nguyen, Q. Luu, and B. Di Bartolo, *J. Lumin.* **85**, 295 (2000).
- ³⁶E. Nakazawa, *J. Lumin.* **12/13**, 675 (1976).
- ³⁷T. Riedener, H. U. Güdel, G. C. Valley, and R. A. McFarlane, *J. Lumin.* **63**, 327 (1995). Tm³⁺ is known to show upconversion luminescence upon excitation of Yb³⁺ as a sensitizer.³⁷ We do not observe any Tm³⁺ upconversion luminescence in YGG:2% Cr³⁺, 1% Yb³⁺ and YGG:1% Yb³⁺. Therefore, we can unambiguously exclude an involvement of Tm³⁺ in the upconversion behavior of YGG:2% Cr³⁺, 1% Yb³⁺.
- ³⁸N. Bloembergen, *Phys. Rev. Lett.* **2**, 84 (1959).
- ³⁹V. V. Ovsyakin and P. P. Feofilov, *Zh. Eksp. Teor. Fiz.* **4**, 471 (1966) [*Sov. Phys. JETP Lett.* **3**, 317 (1966)].
- ⁴⁰M. Yamaga, B. Henderson, K. P. O'Donell, and G. Yue, *Appl. Phys. B* **51**, 132 (1990).
- ⁴¹A. Suchocki *et al.*, *J. Alloys Compd.* **225**, 559 (1995).
- ⁴²M. P. Hehlen, G. Frei, and H. U. Güdel, *Phys. Rev. B* **50**, 16 264 (1994).
- ⁴³B. Struve and G. Huber, *Appl. Phys. B* **36**, 195 (1985).
- ⁴⁴E. I. Solomon and A. B. P. Lever, *Inorganic Electronic Structure and Spectroscopy* (Wiley-Interscience, New York, 1999), Vol. 1, Chap. 5.
- ⁴⁵R. Knochenmuss, Ch. Reber, M. V. Rajasekharan, and H. U. Güdel, *J. Chem. Phys.* **85**, 4280 (1986).
- ⁴⁶O. S. Wenger and H. U. Güdel, *J. Chem. Phys.* **114**, 5832 (2001).